ELSEVIER

Evaluation of transversal and longitudinal dispersion in a flow injection system by exploiting laser induced fluorescence: influence of flow-cell positioning

Cristina M. Quintella[a,*], Yuji N. Watanabe[a], Angelo M.V. Lima[a],
Mauro Korn[b], Iuri Pepe[c], Marcelo Embiruçu[d], Ana Paula S. Musse[a]

[a] *Instituto de Química, Universidade Federal da Bahia, 40170-290 Salvador, BA, Brazil*
[b] *Departamento de Ciências Exatas e da Terra, Universidade do Estado da Bahia, Brazil*
[c] *Instituto de Física, Universidade Federal da Bahia, Brazil*
[d] *Escola Politécnica, Universidade Federal da Bahia, Brazil*

Abstract

A fully mechanized set-up was built for the experimental determination of bi-dimensional dispersion with high spatial resolution ($2400 \, \mu m^2$). Gravitational and wall effects in a single stream were evaluated by using time-based sampling and a micro-flow cell. Vertical upward and downward flows as well as horizontal flows were investigated. Ethylene glycol (MEG) and Rhodamine B in MEG were used as carrier and sample solutions, respectively. Longitudinal profiles were obtained by laser induced total fluorescence (LIF) at up to 19 transversal sites and combined to generate high-resolution bi-dimensional profiles. A two frontal maxima pattern was observed for all flows. The volumetric fraction of RB shape was highly stretched for downward flow and there was high asymmetry for horizontal flow. The sensitivity of three dispersion parameters was evaluated: maximum peak value, peak half-width at half-height, and peak area.

Data modeling showed that the tanks-in-series was more sensitive to wall effects, had good adjustment with only one tank for upward and horizontal flow and needed two tanks for downward flow which was attributed to the latter having higher dispersion. A black box empirical modeling described better the gravitational effect and allowed to identify a parameter sensitive to upward and downward flow as well as hinting to two inner streams within the horizontal flow. It also pointed to a wall dispersion contribution of twice that of the liquid–liquid dispersion.

1. Introduction

Flow injection systems [1] rely on sample/reagents dispersion. From the viewpoint of molecular hydrodynamics, dispersion is the macroscopic evidence of the mutual molecular permeation of two or more liquids (either mass transport or molecular diffusion). Dispersion controls the interaction between carrier, reagent and sample solutions, and leads to intermolecular interactions and chemical processes like reactions. This is the case in liquid–liquid [2,3] and solid–liquid extraction [4], sample dilution [5], column chromatography [6], nanodevices [7] and capillary electrophoresis [8].

Since the beginning of flow injection analysis dispersion has been a concern among researchers, as it has been always recognized as the most relevant parameter for increasing reaction yields and analytical throughput [5]. Within an unsegmented flow system, dispersion takes place both along (longitudinal or axial dispersion) and across (transversal or radial dispersion) the flow direction.

* Corresponding author. Tel.: +55 71 99363126; fax: +55 71 2355166.
E-mail address: cristina@ufba.br (C.M. Quintella).

Longitudinal dispersion has been exhaustively investigated and there are numerous texts reporting its dependence on the main experimental parameters (injection type, sample volume flow rate, analytical path length, reactor geometry, detection cell characteristics, analyte molecular diffusion coefficient, occurrence of chemical reactions, etc.) [9–14]. Earth's gravitational acceleration affecting dispersion in analytical flow systems has not yet been reported. It has been found that the coils spatial orientation affects the retention of high-density particles [4]. Murugaiah et al. [15] reported an experimental study of transversal dispersion based on radial dispersion profiles obtained by refractive index optics. Data were obtained perpendicularly to the flow direction and averaged over a 10 mm longitudinal flow-cell length. The pioneering nature of the work should be emphasized, but the measurements were characterized by low longitudinal resolution and were obtained at only three transversal sites. Concerning high-resolution bi-dimensional experimental determinations of dispersion, it seems that no information is available in the literature.

The viscosity effect was previously reported by Li et al. [16] who observed that the peak shapes were dependent on the sample and reagent injection sequence. They attributed this bulk effect to the different chemical diffusivity of the chemical species within solutions.

Dispersion depends not only on the geometry of the flow system, experimental parameters and bulk interactions but also on wall interactions. For micro-flow cells (MF-cells), boundary layers are usually thicker than expected from traditional fluid mechanics [17], leading to a more pronounced wall drag; chemical processes become then dominant.

At the tube walls, dispersion depends on the solid–liquid interfacial tension (Γ_{SL}). Static Γ_{SL} can be determined by sessile drop contact angle (θ_c) measurements [18]. There is a causal relationship between $\cos \theta_c$ and interfacial chemical groups at the interface, as well as their relative orientation [19-22]. A novel method to observe the relative dynamic Γ_{SL} for liquids flowing on solid surfaces is being recently developed [22–25].

The aim of this work was to evaluate experimentally—with high-resolution—both transversal and longitudinal dispersion in a flow injection system. For this task, a fully mechanized system was designed. High-resolution bi-dimensional measurements of sample total fluorescence were carried out within the carrier slices. In order to lessen the reagents dispersion within the bulk, ethylene glycol (MEG), a liquid with dynamic viscosity 23 times higher than water [26] was used as matrix for the sample and carrier stream. The materials used for building-up the analytical path and flow cell were chosen in order to increase the dispersion caused by liquid-wall drag. The effects of gravity dispersion due to different flow orientations (horizontal and vertical upward or downward) were also investigated. Data were modeled by using either an empirical black box model or a theoretical tanks-in-series model.

2. Black box and tanks-in-series models

Several theoretical models have been proposed to describe dispersion on both general and specific flow systems, as emphasized in comprehensive reviews by Hull et al. [27] and Kolev [28]. Models for bi-dimensional dispersion, including longitudinal and transversal dispersions [13,29] generally predict parabolic profiles. Here an empirical (black box) and a deterministic (tanks-in-series) model were selected.

For the black box empirical model, the longitudinal dispersion profiles are initially fitted to Eq. (1) through the least-squares approach

$$F(t) = \alpha(e^{-\beta_1 t} - e^{-\beta_2 t}) \tag{1}$$

where t is the time elapsed and α, β_1 and β_2 are the empirical parameters of transversal dispersion. This presented three or more maxima and were modeled by fitting a sum of Gaussians, as previously described [17]:

$$F(r) = y_0 + \sum_{i}^{n} G_i(r) \tag{2}$$

where G is the Gaussian function, r the radial coordinate, y_0 the data offset, and n the number of Gaussians required for proper data fitting.

For the analytical deterministic model of tanks-in-series is used a lumped parameter approach. The following equation is fitted to the longitudinal dispersion profiles:

$$F(t) = k_c(r) \left\{ 1 - e^{-t/\tau(r)} \sum_{i=1}^{N} \left[\frac{t/\tau(r)}{(i-1)!} \right] \right\} + c(r) \tag{3}$$

where k_c is the constant (gain), τ the time constant, r the radial coordinate and N the number of tanks.

For transversal dispersion one of the possible equations was proposed by Taylor [30]:

$$h(x, r, t) = h_m(x, t)$$
$$+ \frac{b^2 u}{4 D_m} \left[-\frac{1}{3} + \left(\frac{r}{b} \right)^2 - \frac{1}{2} \left(\frac{r}{b} \right)^4 \right] \frac{dh_m(x, t)}{dx} \tag{4}$$

where h_m is the average concentration in the cross-section of the flow, b the tube radius or half a channel height (m), h the concentration (mol m^{-3}), r the radial coordinate, t the time, D_m the molecular diffusion coefficient (m^2 s^{-1}) and x the distance in a Cartesian coordinate system (m).

3. Experimental

3.1. Reagents and solutions

The carrier fluid was ethylene glycol (MEG) from Synth (99.5% purity) with viscosity and density of 21 mPa and 1.11 g cm^{-3} at $24.5 \pm 0.5\,^\circ$C.

As water is much less viscous than MEG, bulk dispersion with MEG is lower. On the other hand, the static solid–liquid

interfacial tension between borosilicate glass and water is higher in relation to MEG, as determined by θ_c [22]. This makes MEG more suitable to study dispersion as not only interfacial processes become less pronounced, but also bulk dispersion becomes lower, thus easier to be observed. Rhodamine B (RB) from Merck (99.9% purity), dissolved in MEG was used to mimic the sample due to its current usage as a fluorescent probe and its high diffusion in the carrier. The $1.25 \times 10^{-3}\,\text{mol}\,\text{L}^{-1}$ RB solution had density of $1.12\,\text{g}\,\text{cm}^{-3}$ and the viscosity was 13% lower than pure MEG. The RB concentration was chosen to avoid fluorescent aggregates that can serve as additional acceptors of the excitation energy and favor non-radiative excitation transport [31]. For the established temperature, RB dissolved in MEG only dimerizes at concentrations above $1 \times 10^{-2}\,\text{mol}\,\text{L}^{-1}$ [32]. This value is two orders of magnitude higher than in water or methanol, which was attributed to much stronger electrostatic repulsion between the positively charged moieties in MEG. Förster non-radiative energy transfer has a critical radius of $\sim$55 Å [33], thus RB molecules should be, on average, further apart (ca. 75 Å) than this value.

The optical path length of the MF-cell was low enough to avoid secondary effects on the fluorescence quantum yield and the laser power was low enough to avoid transition saturation. The total fluorescence signal was obtained as a function of RB concentration and laser power. The operating conditions of the system were well within the linear region for both parameters. RB concentration was chosen in order to satisfy all constraints for the fluorescent probe (sample solution), yet still providing a high signal-to-noise ratio for the total fluorescence measurements. No degradation of the dissolved RB due to the laser energy was observed for the liquid flow.

Fluorescence from dye adhering to the tubing inner wall or present in the boundary solvent layer may differ from that of dye molecules in the bulk liquid. However, the contribution from fluorescence due to RB interacting directly with the inner walls of the MF-cell did not exceed 1×10^{-5} (0.001%). This estimate is based on an assumed thickness of the boundary solvent layer of $2\,\text{Å} \times 25\,\text{Å}$ and an optical path length ranging from 1 mm at the center of the MF-cell to 0.47 mm at its borders. Absorption spectra obtained prior and after the experiments showed that there was no remaining RB retained on the MF-cell surface.

3.2. Apparatus

Fig. 1 (top) schematizes the flow manifold designed in the single line configuration and involving time-based injection [34] with two Neptune Research 161K031 three-way solenoid valves (V_1 and V_2) to select the sample (S) and carrier (C). The carrier (or sample) solution was aspirated at $5.12\,\text{mL}\,\text{min}^{-1}$ ($10.9\,\text{cm}\,\text{s}^{-1}$) by a four-channel Gilson MP4 peristaltic pump (Pp).

Contact angles (θ_c) were determined in order to choose materials for tubes that maximize the contribution of Γ_{SL} to
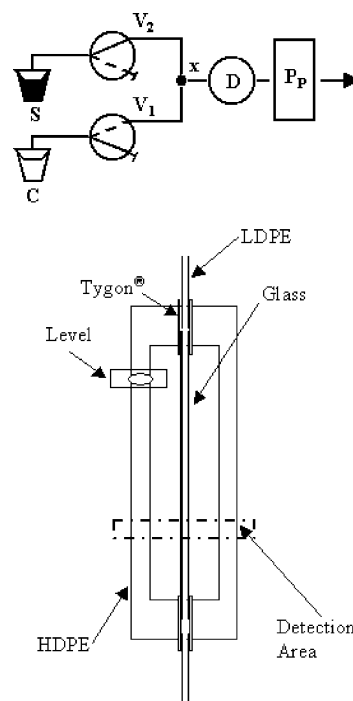

Fig. 1. Top: flow manifold; bottom: micro-flow cell (MF-cell); C: carrier; S: sample; V_i: solenoid valves; x: confluence; D: MF-cell; P_P: peristaltic pump.

dispersion due to interaction with the walls. The relative interfacial interaction for chemical constituent of the tube was evaluated in terms of the cosine of its contact angles ($\cos\theta_c$) with MEG. When $\cos\theta_c$ increases, capillary and wetting efficiency increase in the same proportion [18], increasing dispersion at the borders of the tube.

PTFE® and low-density polyethylene (LDPE) presented high flexibility and θ_c of 68° and 76°, respectively. Tubing of these materials were then selected for building-up the manifold. LDPE has a $\sim$58% higher $\cos\theta_c$ and, consequently, higher capillarity. It presents also low wall permeability to air in contrast to PTFE®, which led to production of air bubbles. As the objective was to map the initial dispersion, the analytical path was chosen as very short and the used LDPE tubing was not coiled. It should be stressed that straight tubes have been often used in investigating dispersion in unsegmented flow analysis. Here, a 30 cm long LDPE tube with an inner diameter of 0.8 mm was used.

The MF-cell (Fig. 1, bottom) consisted of a 7.5 cm borosilicate tube with an inner diameter of 1.0 mm. Although the diameters of flow injection manifolds are presently two or three times lower relatively to this diameter, the high MEG viscosity and the 0.055 mm data acquisition resolution improved the visualization of the dispersion, since the facial velocity is reduced in the MF-cell.

Borosilicate was chosen in view of its high optical transparency within the working spectral range. It presented an angle of contact of 18° with MEG thus it induces pronounced dispersion at the walls. The output and input LDPE tubes
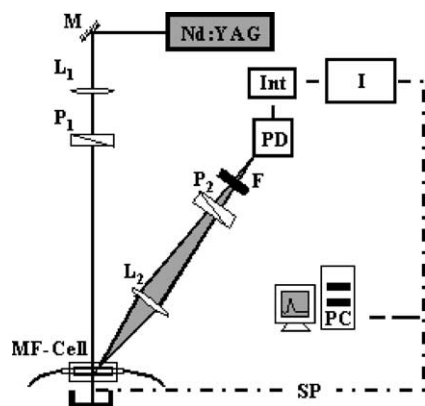
Fig. 2. Experimental set-up. Nd:YAG: laser; M: mirror; L_i: lenses; P_i: polarizers; MF-cell: micro-flow detection cell; F: cut-off filter; PD: photodiode; Int: integrator; I: interface; PC: personal computer; SP: sample positioning system.

were connected to the MF-cell by means of two cylindrical sleeves of high-density polyethylene (HDPE).

The tube length was multiplied by $\cos \theta_c$ of the material in order to evaluate the relative contribution to dispersion due to interfacial phenomena of the tube walls [22]. The LDPE analytical path region had a ~2.4-fold higher contribution to dispersion, due to Γ_{SL}, than the glass MF-cell.

Fig. 2 shows the optical set-up for laser induced total fluorescence [25]. Briefly, a 532 nm Nd:YAG laser beam (Continuum Surelite SLII-10), at 0.55 mJ per pulse and 10 Hz, was deflected by mirror M and focused by lens L_1 into the sample, on a 55 µm diameter spot. A vertical polarizer P_1 ensured 100% polarization. Fluorescence was collected by lens L_2, at 40° to the incident laser beam, and passed through a 550 nm cut-off filter F to block laser radiation. Polarizer P_2 selected fluorescence polarization. Fluorescence was collected at detector PD from a solid angle of 0.02 sr. This detector, of in-house construction, consisted of a RS-Electronics BPW-21 photodiode with 7.5 mm^2 of active area operated as a current-to-voltage converter with seven optional sensitivity ranges.

3.3. Procedure

One 85 ± 1 µL of sample plug was introduced in the carrier stream for 1.00 s.

The initial vertical and horizontal positions of the MF-cell were adjusted with a bubble level (Fig. 1, bottom) and confirmed by laser back-scattering. Detection started 50 mm after the sample zone entered the MF-cell.

The MF-cell position was uniformly varied in relation to the laser beam by a two-axis translation frame [23] with two stepping motors remotely controlled through a QUICK BASIC 4.5 software, permitting sample positioning and real-time data acquisition with mechanical repeatability better than 0.1%. The MF-cell was scanned by fixing its position and, at each transversal position (x), by acquiring fluorescence peaks as a function of time with a synchronized sample plug flowing inside the cell.

The PD output was connected to a data acquisition and control interface (I) and controlled by a personal computer (PC).

The interface was developed for the parallel printer port. It consisted of two 12 bit ADCs (ADS 7804 from Burr Brown with 5.7 µs conversion time), two-step motor control units and one four-channel micro-valve control unit. Sample and carrier input valves (V_1 and V_2 in Fig. 1, top) as well as the data acquisition were synchronized by the acquisition software. The initial time was tagged by the pump duty cycle by an in-house developed optical encoder, mounted on the head of the pump, and connected to the interface.

As ethylene glycol is a high viscous solvent compared to water, there is an increase in the fluorescence lifetime of the probe [35,36]. The laser pulse has a half-width of 7 ns and the probe fluorescence lifetime is ~5 ns under these experimental conditions [37]. An active area RC low filter (Int) was built to integrated the fluorescence signal with a time constant covering about 10 laser pulses (ca. 1 s).

As a consequence of the cylindrical shape of the MF-cell and front-surface fluorescence collections (Fig. 2), some laser light scattered along the detection axis when scanning vertical flows off center in the cell. Because filter F eliminated only 75% of the laser light, errors in polarization were noted. In order to compensate this effect, the signal was acquired with the MF-cell empty. After correction, vertical profiles were found to be similar for both sides of the tube. The data presented here correspond to duplicated half tube scans.

Each fluorescent profile was obtained at least three times and then averaged in order to reduce random noise.

Data modeling employed the softwares MathLab 6.5 and Origin 6.1.

4. Results and discussion

On a first approximation, there are three possible independent contributions to dispersion: the gravity, the walls drag and the difference of viscosity between MEG and RB solution.

For downward vertical flow, gravity is against the pump impulsion whereas for upward flow it cooperates; for horizontal flow, the walls drag is perpendicular to both gravity and pump impulsion. In this work, the flow system operates at a constant averaged flow rate; therefore variations in dispersion can be attributed mainly to the combined effects of earth's gravitational field and wall drag propagation. As the densities of the sample and carrier solutions varied in less than 0.1%, gravitational effects were assumed to be similar for both.

By considering the flow systems and MF-cell as an infinite tube [38] the Reynolds number is <7. Laminar flow is then fully established at 20 mm, as the tube was 50 times longer than wide. This is consistent with a boundary layer with a persistence length of 0.6 mm, i.e., wider than the mean MF-cell radius. Thus, the flow consisted mainly of boundary layer
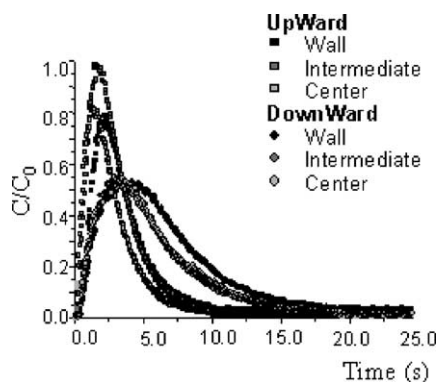
Fig. 3. Concentration profiles for vertical flow at three transversal positions.

where fluid dynamic equations cannot be straightforward applied as the chemical interactions dominate [17].

Interfacial interaction due to capillarity at the tube walls yields a drag that propagates throughout the liquid and slows downstream at any direction. As the RB solution was 13% less viscous than MEG, it becomes less sensitive to flow changes caused by wall drag propagation.

Some LIF profiles are presented in Fig. 3 which shows that for downward flow, dispersion was clearly lower than for upward flow. In situations of horizontal flow, RB solution is mainly at the bottom half of the MF-cell.

The averaged profiles, obtained at up to 19 transversal positions, were juxtaposed in bi-dimensional maps of sample distribution (Fig. 4).

The parameters related to dispersion were evaluated for different flow geometries and are presented in Table 1. Intrinsic total fluorescence (C_0), corresponding to maximum sample concentration, was determined under steady state conditions, by passing only RB solution in the flow system. The increase of the probe dispersion causes D, A and W to increase.

It is possible to infer that for downward flow, dispersion is always higher than for upward flow, regardless of the considered parameter. This is also evident in Fig. 4A and B. The wall
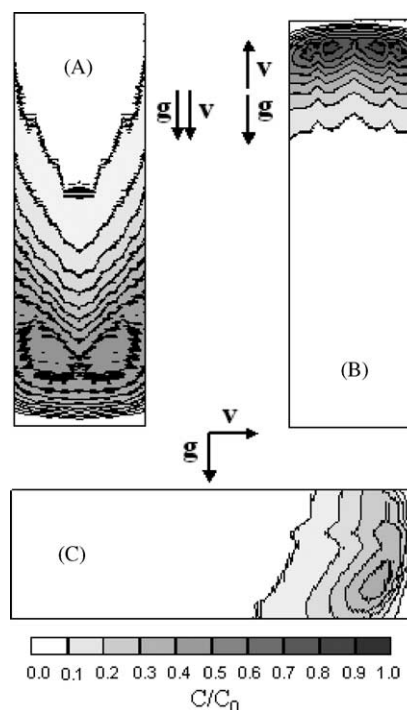

Fig. 4. Sample distribution maps of normalized laser induced total fluorescence (LIF) obtained by juxtaposing longitudinal dispersion profiles, showing direction of flow velocity (v) and of gravity (g): (A) downward flow; (B) upward flow; (C) horizontal flow.

effect for downward flow increased at the wall neighborhood in about 4, 24 and 17% for D, W and A, respectively.

Sample distribution maps for both downward (Fig. 4A) and upward flows (Fig. 4B) exhibited two maxima at the front portion of the sample zone, suggesting annular flow. The two-maxima pattern of transversal dispersion was theoretically predicted by random walk simulation for a similar flow system [13] at low reduced dispersion times, i.e., for short analytical paths, as in the present situation. For upward flow, D is more sensitive to annular flow, as no dispersion is noted at the wall intermediary transversal position (D,

Table 1

Dispersion parameters obtained for vertical flow (upward and downward) and for horizontal flow, acquired at three transversal positions (x)

	Dispersion								
	D (C_0/C)			W (s)			A (Counts s)		
	Center	Intermediary	Near the wall	Center	Intermediary	Near the wall	Center	Intermediary	Near the wall
Vertical flow									
Upward flow	1.2	1.0	1.3	56	58	61	57	72	76
Downward flow	1.8	1.8	1.9	116	114	144	78	77	91
Downward/upward	1.5	1.8	1.5	2.1	2.0	2.4	1.4	1.1	1.2
	Bottom wall		Bottom intermediary		Center		Top intermediary		Top wall
Horizontal flow									
D	1.5		1.3		1.7		1.9		2.2
W	51		48		45		45		45
A	46		48		36		30		25

C: maximum peak value; C_0: maximum peak value of concentrated solution; W: half-width at medium height; A: peak area.

1.0). For downward flow, D becomes least influenced by wall vicinity.

The concentration profile of RB solution is flatter at the front relatively to the trailing edge (Fig. 4A–C). This is a consequence of the viscosity effect. The lower viscosity of RB solution, when compared to MEG, reduces the liquid molecules cohesion, increasing the MEG efficiency to deform the RB solution intermolecular bond network and favoring MEG permeation through RB solution. MEG penetration at the center of the RB zone increases the transversal dispersion significantly. This effect explains the appearance of two lateral maxima typical of annular flow.

Parameter A is sensitive to central penetration (fluid dynamical tunneling effect) of the RB solution by MEG. At the intermediary region, A values were similar to the values near the wall for upward flow and to the central values for downward flow. This is explained by the penetration of the RB solution plug by the MEG plug being more efficient for the downward flow.

The cell positioning effect can also be observed when horizontal flow is concerned. There is a higher sample concentration in the bottom half of the MF-cell, causing W and A to increase and D to decrease. D is lowest at the bottom intermediary position where lies the maximum concentration. W is sensitive to dispersion only for the bottom half, increasing with the vicinity of the wall. A is highest at the bottom intermediary position where lies the maximum concentration. For horizontal flow, the sum of the longitudinal profiles areas acquired at the MF-cell bottom was about 75% of the sum of all the profiles probably due to the gravitational effect.

At the top of the tube, the downward pull of gravity opposed the effect of interfacial tension (Γ_{SL}), thus lessening drag at the interface and increasing it at the bottom wall. The decreased drag at the top wall caused its propagation throughout the liquid to be lower relatively to the bottom wall, and RB solution molecules tend to concentrate near the bottom wall. In addition, the lower viscosity of the RB solution compared to MEG, also favors deformation of the sample distribution and penetration of MEG at the top of the flow.

The black box α, β_1 and β_2 empirical parameters were adjusted for different fixed values of transversal position. Then they were modeled as a function of the radial coordinate by applying Eq. (2), and the results are shown in Fig. 5A. For modeling of the transversal dispersion associated to upward and downward flows, only three Gaussians were required whereas for horizontal flow four Gaussians were necessary. Fig. 5B present the maps including both longitudinal and lateral modeled distribution. Table 2 presents the area of the fitted Gaussians for the lateral parameters.

For the empirical black box modeling, it is assumed that the lateral Gaussians represent the region were dispersion depends mainly on the interaction with the tube walls, and that the central Gaussians depend on the liquid–liquid dispersion. From Table 2, it is possible to observe that α is sensitive to the upward and downward movement whereas β_1 and β_2 are not susceptible to this.
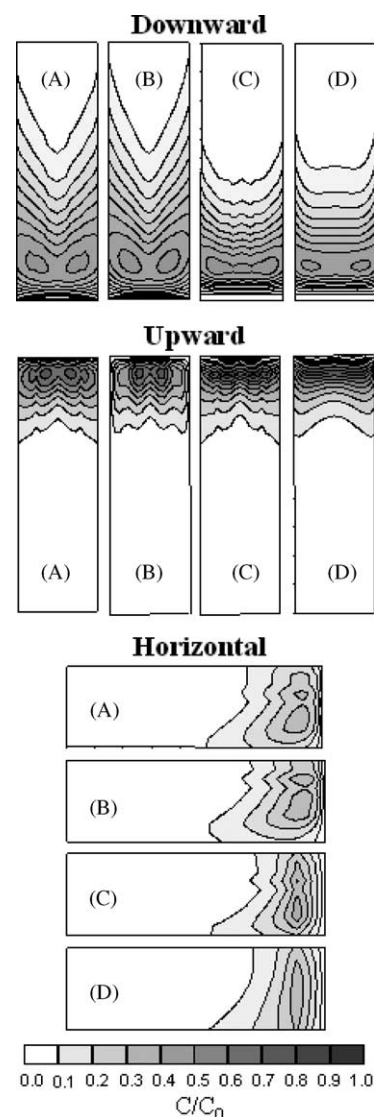

Fig. 5. Theoretical modeled maps for downward, upward and horizontal flows: (A) fitted longitudinal profiles using the black box model; (B) transversal and longitudinal fitted profiles using the black box model; (C) longitudinal adjusted profiles using the tanks-in-series model; (D) both the longitudinal tanks-in-series adjustment and the transversal adjustment using Eqs. (5) and (6).

Wall influence was evaluated by adding the area of the lateral Gaussians. It was similar for β_1 and β_2 (about 70%). For α, it was much higher for upward flow than for downstream flow (about 87 and 45%). Thus, α is quite sensible to wall drag coupling with gravitational effects.

For horizontal flow, the α needed two Gaussians to adjust the central flow, pointing out two different longitudinal streams within the flow. Parameters β_1 and β_2 were quite sensible to wall effects (>90%).

Eq. (3), for similar tanks, was fitted to the longitudinal dispersion profiles acquired at each of the transversal sites. In the present system, k_c is related to the steady situation involving laser signal and sample concentration, and τ is related to the system residence time. The optimum number of tanks

Table 2
Area of the fitted Gaussians (A_g) for the black box model parameters α, β_1 and β_2

	α			β_1			β_2		
	Left	Central	Right	Left	Central	Right	Left	Central	Right
Vertical flow, A_g (%)									
Upward	43	13	43	34	31	34	34	32	34
Downward	22	55	22	33	34	33	36	29	36
Downward/upward	0.52	4.2	0.52	0.97	1.1	0.97	1.1	0.91	1.1

	α				β_1			β_2		
	Top	Middle top	Middle bottom	Bottom	Top	Central	Bottom	Top	Central	Bottom
Horizontal flow, A_g (%)	8	18	54	20	24	6	70	29	08	63

(N) was one for both upward and horizontal flows and two for downward flow, being the latter attributed to its inherent higher dispersion (Fig. 5C).

In order to obtain the transversal dispersion, the obtained dynamical parameters α and β were modeled by using equations derived from Taylor equation (Eq. (4)) for axial dispersion:

(A) Downward and upward vertical flows:

$$k_c(r) = \gamma r^4 + \delta r^2, \qquad \tau(r) = \gamma r^4 + \delta r^2 \qquad (5)$$

(B) Horizontal flow:

$$k_c(r) = \gamma r^2 + \delta r, \qquad \tau(r) = \gamma r^2 + \delta r \qquad (6)$$

Note that for horizontal flow a different equation should be used, due to the non-symmetrical pattern of its radial distribution. Fig. 5D presents the modeled profiles including both longitudinal and transversal contributions. For tanks-in-series, the model does not fit properly [28] as the sample volume is not much lower than the reactor (plus detector) inner volume. In addition, the fluorescence sampling volume is very low.

The relative standard deviation (R.S.D.) associated with the area for each tanks-in-series fitted profile was evaluated with respected to the area of the experimental profiles for vertical and horizontal flows. For only longitudinal adjusted profiles, the R.S.D. of upward and horizontal flows were lower than for downward flow. Further studies may include different tanks in order to improve the model. The inclusion of transversal dispersion modeling increased R.S.D. for upward and horizontal flows and decreased it for downward flow.

5. Conclusions

High-resolution patterns of bi-dimensional reagents dispersion were experimentally determined for MF-cell with downward or upward or horizontal flow.

The pattern with two frontal maxima, at symmetrically transversal positions, was experimentally observed for the first time. For downward flow, the maxima were longitudinally stretched. For horizontal flow the maximum at the top half of the MF-cell was lower.

For downward flow, the dispersion was higher than for upward flow due to opposing wall drag and gravitational forces in the former case. For horizontal flow, could be observed high asymmetry of volumetric fraction of RB shape due to the lower top MF-cell wall drag relative to bottom wall drag.

Sensitivity to transversal dispersion varied for each method of evaluating dispersion. The maximum peak value (M) showed, for vertical flow, high sensitivity half way out from the center. The half-width at half-height (W) showed high sensitivity at the center for vertical flow and at the borders for horizontal flow. The peak area (A) showed, for vertical flow, quite low sensitivity for dispersion at half way out from the center and, for horizontal flow, presented higher sensitivity near the cell borders.

Black box fitting of the experimental data allowed to identify a parameter sensitive to upward and downward flow as well as hinting to two inner streams within the horizontal flow. The parameters β_1 and β_2 point to a wall dispersion contribution of twice that of the liquid–liquid dispersion.

The theoretical modeling with tanks-in-series for longitudinal dispersion had good adjust with only one tank for upward and horizontal flow and needed two tanks for downward flow which was attributed to the latter having higher dispersion. The inclusion of the lateral flow modeling proved convenient for the downward flow and further studies are needed to determine which equations adjust better the other flows.

References

[1] T.K.V. Krawczyk, M. Trojanowicz, N. El-Mur, Lab. Robot. Autom. 12 (2000) 205.

[2] B. Karlberg, S. Thelander, Anal. Chim. Acta 98 (1978) 1.

[3] H.F. Bergamin, J.X. Medeiros, B.F. Reis, E.A.G. Zagatto, Anal. Chim. Acta 101 (1978) 9.

[4] M. Hulsman, M. Bos, W.E. van der Linden, Anal. Chim. Acta 346 (1997) 351.

[5] J. Ruzicka, E.H. Hansen, Anal. Chim. Acta 99 (1978) 37.

[6] D.W. Morton, C.L. Young, J. Chromatogr. Sci. 33 (1995) 514.

[7] B. Bühler, D. Fröhlich, H.M. Haake, A. Brecht, G. Gauglitz, Trends Anal. Chem. 20 (2001) 186.

[8] L. Arce, P. Kuban, A. Ríos, M. Valcárcel, B. Karlberg, Anal. Chim. Acta 390 (1999) 39.

[9] E.B. van Akker, M. Bos, W.E. van der Linden, Anal. Chim. Acta 373 (1998) 227.

[10] J.M. Reijn, W.E. van der Linden, H. Poppe, Anal. Chim. Acta 114 (1980) 105.

[11] J.T. Vanderslice, K.K. Stewart, A.G. Rosenfeld, D.J. Higgs, Talanta 28 (1981) 11.

[12] T. Korenaga, Anal. Chim. Acta 261 (1992) 539.

[13] P.D. Wentzel, M.R. Bowdridge, E.L. Taylor, C. MacDonald, Anal. Chim. Acta 278 (1993) 293.

[14] F.J. Andrade, F.A. Inõn, M.B. Tudino, O.E. Troccoli, Anal. Chim. Acta 379 (1999) 99.

[15] V. Murugaiah, R.E. Synovec, Anal. Chem. 64 (1992) 2130.

[16] J. Li, G. Liu, H. Ma, T. Korenaga, Anal. Chim. Acta 310 (1995) 329.

[17] C.M. Quintella, C.C. Gonçalves, A.P.S. Musse, A.J. McCaffery, Exp. Fluids 35 (2003) 41.

[18] A.W. Adamson, A.P. Gast, Physical Chemistry of Surfaces, 6th ed., Wiley, New York, 1997, Chapter 10.

[19] P.B. Welzel, C. Rauwolf, O. Yudin, K. Grundke, J. Colloid Interf. Sci. 251 (2002) 101.

[20] Z. Yoshimitsu, A. Nakajima, T. Watanabe, K. Hashimoto, Langmuir 18 (2002) 5818.

[21] C.M. Quintella, A.M.V. Lima, C.C. Gonçalves, Y.N. Watanabe, M.A. Schreiner, A.P. Mammana, I. Pepe, A.M. Pizzo, J. Colloid Interf. Sci. 262 (2003) 221.

[22] C.M. Quintella, C.C. Gonçalves, I. Pepe, A.M.V. Lima, A.P.S. Musse, J. Braz. Chem. Soc. 12 (2001) 780, http://jbcs.sbq.org.br/jbcs/2001/vol12_n6/14.pdf.

[23] C.M. Quintella, C.C. Gonçalves, I. Pepe, A.M.V. Lima, A.P.S. Musse, J. Autom. Meth. Manage. Chem. 24 (2002) 31, http://taylorandfrancis.metapress.com.

[24] C.M. Quintella, C.C. Gonçalves, M.T.P.O. Castro, I.M. Pepe, A.P.S. Musse, A.M.V. Lima, J. Phys. Chem. B 107 (2003) 8511.

[25] C.M. Quintella, Â.M.V. Lima, A.P. Mammana, M.A. Schreiner, I.M. Pepe, Y.N. Watanabe, J. Colloid Interf. Sci. 271 (2004) 201.

[26] Revised Released on the IAPS Formulation 1985 for the Viscosity of Ordinary Water Substance, The International Association for the Properties of Water and Steam, Erlangen, Germany, 1997.

[27] R.D. Hull, R.E. Malick, J.G. Dorsey, Anal. Chim. Acta 267 (1992) 1.

[28] S.D. Kolev, Anal. Chim. Acta 308 (1995) 36.

[29] J.T. Vanderslice, A.G. Rosenfeld, G.R. Beecher, Anal. Chim. Acta 179 (1986) 119.

[30] G. Taylor, Proc. R. Soc. London, Ser. A 225 (1954) 231.

[31] T. Föster, Ann. Phys. 2 (1948) 55.

[32] P. Bojarski, A. Matczuk, C. Bojarski, A. Kawski, B. Kuklinski, G. Zurkowska, H. Diehl, Chem. Phys. 210 (1996) 485.

[33] P. Bojarski, A. Jankowicz, J. Lumin. 81 (1999) 21.

[34] B.F. Reis, M.F. Gine, E.A.G. Zagatto, J.L.F.C. Lima, R.A. Lapa, Anal. Chim. Acta 293 (1994) 129.

[35] M. Megens, R. Sprik, G.H. Wegdam, A. Lagendijk, J. Chem. Phys. 107 (1997) 493.

[36] A.D. Kummer, C. Kompa, H. Niwa, T. Hirano, S. Kojima, M.E. Michel-Beyerle, J. Phys. Chem. B 106 (2002) 7554.

[37] A.D. Scully, A. Matsumoto, S. Hirayama, Chem. Phys. 157 (1991) 253.

[38] B.S. Massey, Mechanics of Fluids, 6th ed., van Nostrand, Wokingham, 1989.